Tellus (2007), 59A, 141–154
Printed in Singapore. All rights reserved

TELLUS

Particle transport in horizontal convection: Implications for the "Sandström theorem"

By OLIVIER MARCHAL*, *Woods Hole Oceanographic Institution, Woods Hole, MA 02543, USA*

(Manuscript received 9 January 2006: in final form 16 May 2006)

ABSTRACT

The "Sandström theorem" as interpreted by Jeffreys is that in a flow maintained by a temperature difference, the pathline from the cold region to the warm region must lie below the return path. A formal demonstration of the argument for a rotating fluid requires three assumptions about the relative circulation around a closed material line: (1) the flow is steady, (2) the closed material line is a closed streamline and (3) the work done by friction along the streamline is negative. The argument extends to unsteady flows, thereby relaxing (1–2), if the absolute circulation along the material line is a bounded function of time—a condition that is met for flows with small Rossby number. Its validity for time-periodic two-dimensional flows of horizontal convection is verified numerically. Poincaré sections reveal the presence of chaotic particle transport in these flows, even though the Eulerian velocity fields have a simple time dependence. In spite of chaotic advection, particle motion is in general downwards in the cold region and upwards in the warm region of the fluid, which is consistent with the flow shape envisioned by Jeffreys. This paper gives support to the validity of his argument for the unsteady case and enhances its relevance for the dynamical interpretation of the basic structure of geophysical flows.

1. Introduction

Horizontal convection denotes a flow forced by uneven heating imposed at the surface of the fluid (Stern, 1975). An outstanding question concerns the form of horizontal convection in the ocean forced by the differential heating with latitude by the sun. An early assertion is the "Sandström theorem", which was stated as follows by Defant (1961; p. 491): *A closed steady circulation can only be maintained in the ocean if the heat source is situated at a lower level than the cold source*. The statement as it stands suggests that surface heating and cooling alone cannot maintain a circulation in the ocean as both occur at the same level. This interpretation has inspired numerous recent studies on the energetics of the ocean general circulation (e.g. Munk and Wunsch, 1998; Huang, 1999; Paparella and Young, 2002; Gade and Gustafsson, 2004; Siggers et al., 2004; Wunsch and Ferrari, 2004; Wunsch, 2005).

Jeffreys (1925), however, proposed that the proper inference to draw from the Sandström theorem is that the pathline from the cold region to the warm one in a flow forced by a temperature contrast must lie below the return path. This inference is here referred to as the "Jeffreys argument" in order to avoid confusion with other statements of the theorem (e.g. Sandström, 1916, p. 39; Godske et al., 1957, p. 262; Defant, 1961, p. 491; Dutton, 1986, p. 380). This is done in spite of the possibility that the inference of Jeffreys (1925) and other statements of the theorem are essentially the same result; for example, if "heat source" "cold source" designates a region in the fluid where the moving fluid is heated (cooled), then his argument and the statement of Defant (1961) would be similar assertions (see the short discussion between Godske, 1936 and Jeffreys, 1936).

In this paper we undertake an analysis of the Jeffreys argument. Jeffreys (1925) remarked that his argument is "an important proposition, and one worth definite proof". Experimental evidence for his argument is suggested in laboratory experiments of a fluid differentially heated from above or below (e.g. Wang and Huang, 2005). However, whereas the paper of Jeffreys (1925) is often quoted as a criticism to an earlier statement of the Sandström theorem (by not considering the effect of heat conduction), we have not been able to find a detailed discussion of his reinterpretation of it in the literature.

The present paper is organized as follows. Section 2 reviews the theoretical basis of the Sandström theorem as originally formulated. First, the case of steady rotating flows is considered. Further development shows how the argument can be simply extended to the unsteady case, thereby enhancing its relevance for geophysical flows. In Section 3, the argument is tested numerically for the simple case of time-periodic two-dimensional (2-D) horizontal convection. The transport of fluid particles is characterized in flows obtained from the numerical integration of the equations of motion. A summary follows in Section 4.

*Correspondence.
e-mail: omarchal@whoi.edu
DOI: 10.1111/j.1600-0870.2006.00193.x

2. Theory

In this section we review the original theoretical foundation of the Sandström theorem (e.g. Defant, 1961; Dutton, 1986). The foundation is provided by the governing equation for the circulation as perceived in a reference frame that is rotating with the planet. The circulation is the integral of the vector velocity $\mathbf{u}$ around an arbitrary closed contour c in the fluid:

$$\Gamma = \oint_c \mathbf{u} \cdot d\mathbf{r}. \tag{1}$$

Here $d\mathbf{r}$ is a line element of c and $\mathbf{u}$ is the relative velocity, that is, the velocity as described in the non-inertial (rotating) frame. The governing equation for Γ is an expression for the rate of change of Γ for the case where the contour c is a closed material line m:

$$\frac{d\Gamma}{dt} = \oint_m \frac{D\boldsymbol{u}}{Dt} \cdot d\boldsymbol{r} + \oint_m \boldsymbol{u} \cdot \frac{d}{\mathrm{d}t}(d\boldsymbol{r}). \tag{2}$$

Here $D\mathbf{u}/Dt = \partial\mathbf{u}/\partial t + \mathbf{u} \cdot \nabla\mathbf{u}$ is the material derivative. For a material line, $d/dt(d\mathbf{r}) = d\mathbf{u}$ so that the integrand of the second term on the right-hand side of eq. (2) is $\mathbf{u} \cdot d\mathbf{u} = d|\mathbf{u}|^2/2$. This term is an integral around a closed contour of an exact differential and, therefore, vanishes. The rate of change $d\Gamma/dt$ is thus directly obtained by integrating the momentum equation around the material line m:

$$\frac{d\Gamma}{dt} = -\oint_m (2\boldsymbol{\Omega} \times \mathbf{u}) \cdot d\mathbf{r} - \oint_m \frac{dp}{\rho} + \oint_m \mathbf{F} \cdot d\mathbf{r}, \tag{3}$$

where $\boldsymbol{\Omega}$ is the angular velocity of Earth rotation, p is the pressure, ρ is the density, and $\mathbf{F}$ is the non-conservative (friction) force per unit mass. Thus, the rate of change of the circulation around m is equal to the sum of the line integrals of the Coriolis, pressure and friction forces along m. A physical interpretation of each term of the right-hand side of eq. (3) can be found, for example, in Pedlosky (1987).

2.1. *Steady flow*

A formal expression of the Sandström theorem and of its interpretation by Jeffreys (1925) arises as an approximation to the complete circulation equation (3). Whereas most of the material here can be found in earlier work (e.g. Dutton, 1986), the present discussion emphasizes the various assumptions (three) underlying the derivation of this expression. In doing so the limitations of this expression for the interpretation of geophysical flows are clarified. Consider the rate of change

$$\frac{d\Gamma}{dt} = \oint_m \frac{D\mathbf{u}}{Dt} \cdot d\mathbf{r}. \tag{4}$$

A first assumption is that the flow is steady ($\partial\mathbf{u}/\partial t = 0$). Under this assumption, the material derivative $D\mathbf{u}/Dt = \mathbf{u} \cdot \nabla\mathbf{u}$. A vector identity allows us to express the advective acceleration as $\mathbf{u} \cdot \nabla\mathbf{u} = \nabla|\mathbf{u}|^2/2 + \boldsymbol{\omega} \times \mathbf{u}$, where $\boldsymbol{\omega} = \nabla \times \mathbf{u}$ is the relative vorticity. Thus, for a steady flow, the rate of change of the circulation around m is

$$\begin{aligned}\frac{d\Gamma}{dt} &= \oint_m \nabla\left(\frac{|\mathbf{u}|^2}{2}\right) \cdot d\mathbf{r} + \oint_m (\boldsymbol{\omega} \times \mathbf{u}) \cdot d\mathbf{r} \\ &= \oint_m d\left(\frac{|\mathbf{u}|^2}{2}\right) + \oint_m (\boldsymbol{\omega} \times \mathbf{u}) \cdot d\mathbf{r} \\ &= \oint_m (\boldsymbol{\omega} \times \mathbf{u}) \cdot d\mathbf{r}.\end{aligned} \tag{5}$$

A second assumption is that the closed material line m is a closed streamline s, that is, $d\mathbf{r} = \lambda\mathbf{u}$, where λ is a coefficient of proportionality, say positive, for each element of the material line. Note that this assumption has a restricted validity: whereas fluid particles follow closed trajectories in a steady incompressible 2-D flow, they do not generally do so in a steady 3-D flow (e.g. Lichtenberg and Lieberman, 1983). A first consequence of this assumption is that the rate of change of the circulation around $m \equiv s$ vanishes, that is,

$$\oint_s (\boldsymbol{\omega} \times \mathbf{u}) \cdot \lambda\mathbf{u} = 0. \tag{6}$$

A second consequence is that the line integral of the Coriolis force around $m \equiv s$ is also zero,

$$-\oint_s (2\boldsymbol{\Omega} \times \mathbf{u}) \cdot \lambda\mathbf{u} = 0. \tag{7}$$

In physical terms, the Coriolis force does not *work* along a streamline, as this force always acts in a direction normal to $d\mathbf{r} = \lambda\mathbf{u}$. With the two assumptions above, the equation for the circulation around $m \equiv s$ is

$$0 = -\oint_s \frac{dp}{\rho} + \oint_s \mathbf{F} \cdot d\mathbf{r}. \tag{8}$$

Thus, the work done by the pressure force must balance the work done by the friction force along a closed streamline in a steady flow. A balance identical to eq. (8) can be found, for example, in Defant (1961) and Dutton (1986).

The final assumption involves the frictional work $\oint_s \mathbf{F} \cdot d\mathbf{r}$. Previous authors took for granted that $\oint_s \mathbf{F} \cdot d\mathbf{r}$ is necessarily negative. To investigate this consider the important case of a Newtonian fluid with constant kinematic viscosity ν. The friction force per unit mass for such a fluid is $\mathbf{F} = \nu\nabla^2\mathbf{u} + (\nu/3)\nabla(\nabla \cdot \mathbf{u})$ (e.g. Batchelor, 1967). Using the vector identity $\nabla^2\mathbf{u} = \nabla(\nabla \cdot \mathbf{u}) - \nabla \times \boldsymbol{\omega}$, this force can be written as $\mathbf{F} = (4\nu/3) \nabla(\nabla \cdot \mathbf{u}) - \nu(\nabla \times \boldsymbol{\omega})$. The integral around a closed contour of the first term on the right-hand side vanishes, so that the frictional work around a closed streamline is

$$\oint_s \mathbf{F} \cdot d\mathbf{r} = -\oint_s \nu\,(\nabla \times \boldsymbol{\omega}) \cdot d\mathbf{r}. \tag{9}$$

The physical mechanism involved in this work is best illustrated for a rectangular coordinate system, such that $\boldsymbol{\omega} = \hat{x}\omega_x + \hat{y}\omega_y + \hat{z}\omega_z$, with the line element $d\mathbf{r}$ locally parallel to one of the axes of the system, say $\hat{x}$ (Fig. 1). Then, the work done by friction

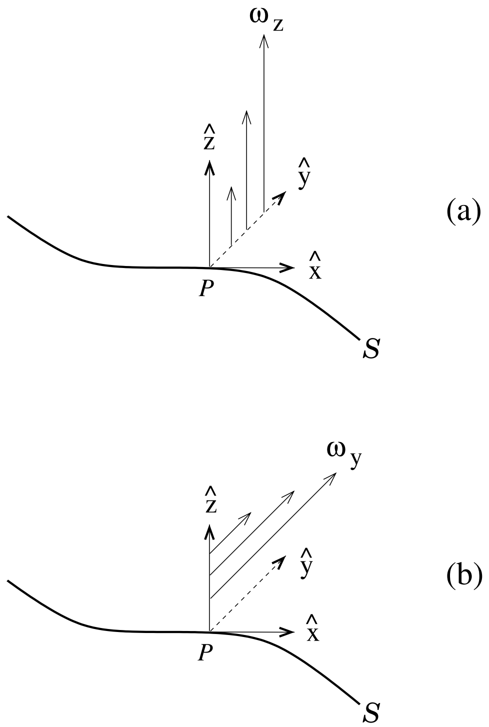

Fig. 1. The two contributions to the work done locally by the friction force along a streamline s, as identified when the unit vector $\hat{x}$ of a rectangular coordinate system is parallel to s (at point P in the figure). These contributions arise (a) from a gradient of the z-component of vorticity along the direction $\hat{y}$ and (b) from a gradient of the y-component of vorticity along the direction $\hat{z}$.

along s is given by

$$\oint_s \mathbf{F} \cdot d\mathbf{r} = -\oint_s \nu \left(\frac{\partial \omega_z}{\partial y} - \frac{\partial \omega_y}{\partial z} \right) dx. \qquad (10)$$

The work done by friction along a streamline s corresponds physically to a diffusion of relative vorticity across s, as for a material line (e.g. Batchelor, 1967). There are separate contributions from diffusion of ω_z down the gradient in the direction $\hat{y}$ (Fig. 1a) and from diffusion of ω_y down the gradient in the direction $\hat{z}$ (Fig. 1b), with due regard for the signs of these contributions to the strength of the circulation around s. Importantly, at the level of the circulation equation, the signs of these contributions and hence the sign of the frictional work $\oint_s \mathbf{F} \cdot d\mathbf{r}$ cannot be determined. Under an appropriate assumption about the vorticity gradients across s, $\oint_s \mathbf{F} \cdot d\mathbf{r}$ is negative, so that $-\oint_s dp/\rho$ must be positive: the moving fluid must expand at high pressures and contract at low pressures.

In summary, the Jeffreys argument can be formalized from three assumptions about the circulation around a material line relative to the rotating Earth: (1) the flow is steady, (2) the closed material line is a closed streamline, and (3) the work done by friction along the streamline is negative. Under these assumptions, the fluid elements moving towards the warm region of the fluid *must* be at higher pressures than the fluid elements moving towards the cold region.

Note that the formal expression of the Jeffreys argument (eq. 8) is different in the Boussinesq approximation (Colin de Verdière, 1993). Under this approximation the work done by the pressure force along a streamline s is nil, that is, $-\oint_s 1/\rho_0 \nabla \tilde{p} \cdot d\mathbf{r} = -1/\rho_0 \oint_s d\tilde{p} = 0$, where ρ_0 is a constant density and $\tilde{p} = p - p_0$ is the pressure difference with respect to the reference state of rest. Work is done instead by the buoyancy force, that is $\oint_s \mathbf{b} \cdot d\mathbf{r} = \oint_s \tilde{\rho}/\rho_0 \mathbf{g} \cdot d\mathbf{r}$, where $\mathbf{b} = \tilde{\rho}/\rho_0 \mathbf{g}$ is the buoyancy and $\tilde{\rho} = \rho - \rho_0$. Expressing gravity as the gradient of a geopotential, $\mathbf{g} = -\nabla\phi$ where $\phi = gz$, the balance (8) becomes

$$0 = -\frac{1}{\rho_0} \oint_s \tilde{\rho}\, d\phi + \oint_s \mathbf{F} \cdot d\mathbf{r}. \qquad (11)$$

In the Boussinesq approximation the Jeffreys argument is that the path towards the warm region of the fluid occurs at lower levels than the return path.

2.2. *Unsteady flow*

We now explore the possible validity of the Jeffreys argument for unsteady flows. Again the circulation eq. (3) is used to provide a theoretical framework. Consider an equivalent expression for the Coriolis term in eq. (3):

$$-\oint_m (2\boldsymbol{\Omega} \times \mathbf{u}) \cdot d\mathbf{r} = -2\Omega \frac{dA_n}{dt}, \qquad (12)$$

where A_n is the equatorial projection of the surface area encircled by the material line. Note that the quantity A_n is considered positive if the sense of integration is counter-clockwise when projected on the equatorial plane (e.g. Godske et al., 1957). The circulation eq. (3) becomes:

$$\frac{d}{dt}(\Gamma + 2\Omega A_n) = -\oint_m \frac{dp}{\rho} + \oint_m \mathbf{F} \cdot d\mathbf{r}. \qquad (13)$$

The sum $\Gamma + 2\Omega A_n$ is the circulation of the absolute velocity $\mathbf{u} + \boldsymbol{\Omega} \times \mathbf{r}$ around m, that is, the circulation as perceived in an inertial reference frame. Averaging eq. (13) in time leads to

$$\frac{\Delta(\Gamma + 2\Omega A_n)}{\Delta t} = -\left\langle \oint_m \frac{dp}{\rho} \right\rangle + \left\langle \oint_m \mathbf{F} \cdot d\mathbf{r} \right\rangle, \qquad (14)$$

where $\langle \cdot \rangle$ denotes an average over the time period Δt. The work done by pressure along a moving material line m is balanced by the frictional work *and* the circulation change along m. For a barotropic inviscid fluid eq. (14) is a formal expression of the Kelvin theorem.

Further progress can be made if the absolute circulation $\Gamma + 2\Omega A_n$ is taken as a bounded function of time. In the geophysical situation boundedness of $2\Omega A_n$ arises as $-2\Omega A_{eq} \le 2\Omega A_n \le 2\Omega A_{eq}$, where $A_{eq} > 0$ is the surface area of the equatorial plane intersected by the planet. In a flow with small Rossby number, $Ro = \mathcal{O}(\boldsymbol{\omega}/2\boldsymbol{\Omega}) \ll 1$, the absolute circulation is dominated by the circulation of the Coriolis force, so that $\Gamma + 2\Omega A_n \sim 2\Omega A_n$

is trivially bounded. In any case, if the absolute circulation is a bounded function of time, the limit of the left-hand side of (14) for $\Delta t \to \infty$ vanishes, so that

$$0 = -\left\langle \oint_m \frac{dp}{\rho} \right\rangle + \left\langle \oint_m \mathbf{F} \cdot d\mathbf{r} \right\rangle. \tag{15}$$

Time averaging for unsteady flow leads, therefore, to a balance that is formally similar to the one derived for steady flow (eq. 8). Provided that a sufficiently long period of time is considered, the work done by pressure and the work done by friction must be equal along a moving material line. Assuming that $\langle \oint_m \mathbf{F} \cdot d\mathbf{r} \rangle < 0$, the Jeffreys argument would then apply in unsteady flows as well.

3. Numerical study

In this section we verify that the Jeffreys argument is valid in unsteady flows for the simple case of time-periodic 2-D horizontal convection. Our motivation is twofold. First, the argument in time-dependent flows assumes that the work done by friction along a moving material line is negative. As for steady flows, that $\langle \oint_m \mathbf{F} \cdot d\mathbf{r} \rangle$ is negative cannot be demonstrated at the level of the circulation equation. The argument requires for its evaluation knowledge about the vorticity field, which can only be obtained from the solution of the full equations of motion with appropriate boundary conditions. Second, that the Jeffreys argument applies also to unsteady flows is not evident given the complex character of Lagrangian transport in such flows. Material lines can be stretched and folded in time-dependent flows (for a review see, e.g. Ottino, 1990). The trajectory of fluid elements in such flows can be chaotic, in the sense of a sensitivity to their initial position in the fluid. Chaotic particle transport can occur even if the Eulerian velocity field has a simple time dependence—a situation called "chaotic advection" (Aref, 1984). For example, particle transport has been shown to become chaotic in a simple (laminar) time-dependent 2-D model of Rayleigh–Bénard (RB) convection (Solomon and Gollub, 1988). This section examines whether the Jeffreys argument applies to time-dependent 2-D horizontal convection when chaotic advection is present.

3.1. Model description

Our approach is based on the characterization of particle transport in flows generated by numerical integration of the equations of motion. A brief description of the numerical model used to generate the flows is given (for details see Appendix A). In this model, motion is confined in the vertical plane, rotation is absent, and the fluid is incompressible and Boussinesq. At the top boundary a condition of no stress and a distribution of temperature are imposed. Unless stipulated otherwise a time-periodic temperature distribution is used. The other boundaries are assumed to be no slip and thermally insulating. Thus, our study extends earlier work with a similar model (e.g. Beardsley and Festa, 1972; Rossby, 1998) by the consideration of time-dependent thermal forcing. This forcing leads to time dependence of the flow in our numerical experiments.

The equations of motion are solved in their dimensionless form, the flow being governed by three dimensionless parameters: the Rayleigh number (Ra), the Prandtl number (Pr), and the aspect ratio of the container. In this paper we consider flows with $Ra = 10^5$, $Pr = 10$, and an aspect ratio of one; the robustness of our results against the value assumed for Ra is touched in Section 4. In spite of its various limitations, the model is thought to capture some of the physics of geophysical flows such as the meridional overturning circulations in the ocean (e.g. Rossby, 1998).

3.2. Steady and unsteady flows

We first consider briefly a numerical experiment with steady horizontal convection. The temperature distribution imposed at the top of the fluid is given by

$$T(x, z=1) = 1 - x, \tag{16}$$

where x is the horizontal coordinate ($0 \leq x \leq 1$) and z is the vertical coordinate ($0 \leq z \leq 1$). The simulated flow exhibits a deep-reaching asymmetric overturning circulation (solid lines in Fig. 2), and the temperature field includes a region of stable (unstable) stratification near the top boundary where maximum (minimum) heating is imposed (dashed lines in Fig. 2). Similar results have been obtained with the same model and discussed in detail in earlier studies (e.g. Beardsley and Festa, 1972; Rossby, 1998). In particular, the asymmetric circulation as simulated by the model has been taken as a numerical illustration of the smallness of the sinking regions in the ocean (e.g. Rossby, 1998).

Note for future reference a simple dynamical interpretation of the simulated circulation that is provided by a balance equivalent to eq. (11). Let $\mathbf{u} = \hat{x}u + \hat{z}w$ be the 2-D flow, where u (w) is the horizontal (vertical) component of velocity. From the Stokes theorem the circulation around a material line in the flow is

$$\Gamma_2 = \iint_A \omega \, dA. \tag{17}$$

Here A is the surface area encircled by the material line and $\omega = \hat{y} \cdot (\nabla \times \mathbf{u})$ is the vorticity of the flow, $\hat{y}$ being a unit vector normal to the plane of motion (subscript "2" for Γ reminds one that eq. 17 refers to a 2-D flow). The governing equation for Γ_2 is

$$\frac{d\Gamma_2}{dt} = Pr\,Ra \oint_m T\,dz + Pr \oint_m \left(\frac{\partial \omega}{\partial z}\,dx - \frac{\partial \omega}{\partial x}\,dz \right). \tag{18}$$

For a streamline s in the steady flow,

$$0 = Ra \oint_s T\,dz + \oint_s \left(\frac{\partial \omega}{\partial z}\,dx - \frac{\partial \omega}{\partial x}\,dz \right). \tag{19}$$

The overturning circulation (Fig. 2) can be interpreted as a balance between the baroclinic production of vorticity generated

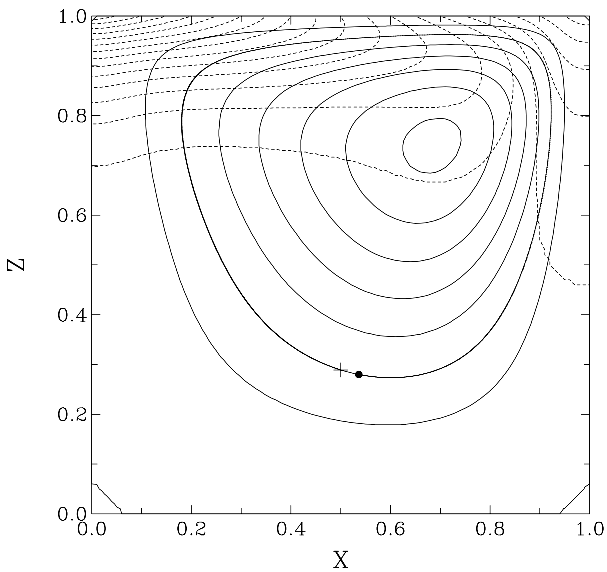

Fig. 2. Fields of the stream function (solid lines) and of the temperature (dashed) in a steady flow of horizontal convection simulated with $Ra = 10^5$ and $Pr = 10$. The aspect ratio of the container is 1. The contour interval is constant in both fields. The accuracy of the finite-difference method used to calculate particle transport is assessed by placing a particle along a streamline ("+" in the figure) and by comparing its pathline with the streamline. The final position of the particle after approximately one revolution in the flow is shown by the solid circle. The pathline and the streamline can hardly be distinguished in the figure.

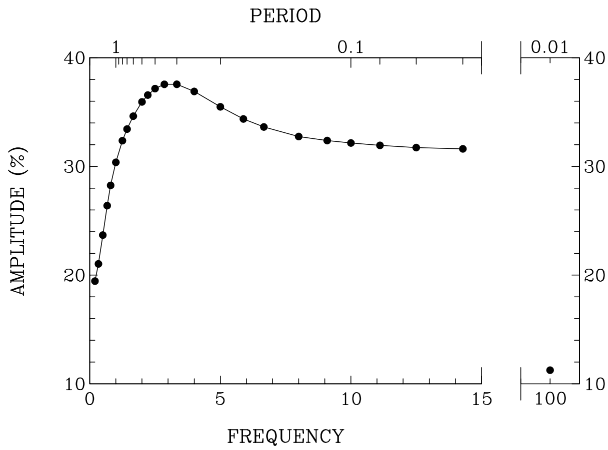

Fig. 3. Sensitivity of the amplitude of the oscillation in flow strength to the frequency of surface thermal forcing in the numerical model of horizontal convection. The flow strength is defined as the maximum stream function in the container ($\psi_{\rm M}$). The amplitude of the flow strength oscillation is defined as $(\psi_{\rm M}^{\rm (max)} - \psi_{\rm M}^{\rm (min)})/\langle\psi_{\rm M}\rangle$, where $\psi_{\rm M}^{\rm (max)}$ ($\psi_{\rm M}^{\rm (min)}$) is the maximum (minimum) of $\psi_{\rm M}$ during one periodic oscillation of the circulation and $\langle\psi_{\rm M}\rangle$ is the mean value of $\psi_{\rm M}$ during the oscillation. Note that the small sensitivity at high frequency suggested by the right tail of the curve does not persist at frequencies >15, as shown by results from one numerical experiment where the frequency (period) of the thermal driving is 100 (0.01).

ultimately by uneven heating at the surface and the diffusion of vorticity across the streamlines.

We now consider a series of numerical experiments of time-dependent horizontal convection. The temperature distribution at the top of the fluid is given by

$$T(x, z=1, t) = (1 - x)(1 + \Delta T \cos(\omega_f t)), \tag{20}$$

where ΔT and ω_f are, respectively, the amplitude and the angular frequency of the thermal forcing. For all numerical experiments $\Delta T = 0.5$. Thus, the imposed temperature at the left end of the container (at $x = 0$) varies from 0.5 to 1.5 with a period $\tau = 2\pi/\omega_f$, whereas the imposed temperature at the right end ($x = 1$) is fixed to 0. A set of numerical experiments illustrates the sensitivity of the flow strength to the forcing frequency over a ω_f-range spanning two orders of magnitude (Fig. 3). For all experiments the flow response is a periodic oscillation (for an example see solid line in Fig. 4a). Interestingly, both high- and low-frequency forcings generate relatively small oscillation amplitudes; maximum amplitude occurs for some intermediate value of ω_f (Fig. 3). Thus, there appears to be a "resonance", over the investigated ω_f-range, of the overturning circulation with respect to the time-periodic thermal forcing that is imposed at the surface.

We examine in more detail the numerical experiment ("reference experiment" hereafter) showing the largest variation in flow strength (38%) in response to the time-varying thermal forcing (with $\tau = 0.3$; Fig. 3). The relation between flow strength and thermal driving (respectively, solid and dashed lines in Fig. 4a) also presents analogies with a weakly damped oscillator subject to a sinusoidal excitation: the periodicity of the flow strength is similar to the periodicity of the thermal driving (in contrast to the oscillator, the time evolution of the flow strength is not sinusoidal) and the flow strength is out of phase with the thermal driving, with maximum strength occurring when the driving is near a minimum and minimum strength preceding maximum driving. The flow structure exhibits also important changes. When the flow strength is maximum the overturning cell occupies approximately the whole container and is centered at a relatively deep level near the middle of the container (Fig. 4b). When the flow strength is minimum, the cell is confined in the upper half of the container and is more asymmetric (Fig. 4c).

We make three comments regarding the circulation responses to the variable thermal forcing (Fig. 3). First, the phase displacement between the thermal forcing and the circulation varies with the forcing frequency (in the case of the oscillator the phase displacement depends on the forcing frequency and on the natural frequency and damping time scale of the oscillator). For example, with the forcing period of 5 (largest period among the experiments reported in Fig. 3), the phase displacement is reduced to ca. 0.6 (12% of the period), that is, the maximum

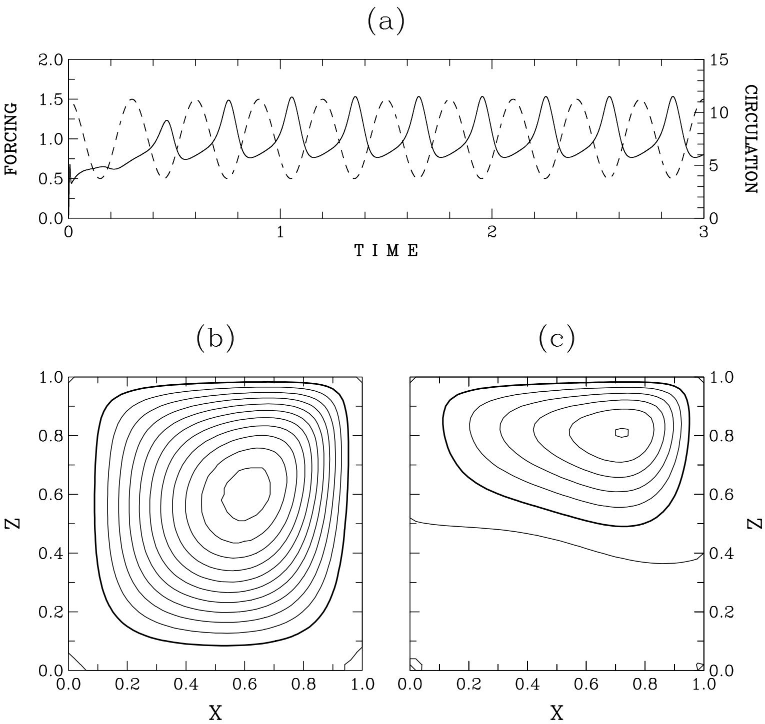

Fig. 4. Results from the numerical experiment showing the largest circulation variability in response to the time-varying thermal forcing at the surface (reference experiment, with $\tau = 0.3$). (a) Time-series of the surface forcing temperature at the left end of the container (dashed) and time-series of the maximum stream function in the container (ψ_{M}, solid). (b) Field of the stream function when ψ_{M} is near its maximum. (c) Field of the stream function when ψ_{M} is near its minimum. In panels (b–c) the thick isoline is for the same value of the stream function for comparison and the contour interval is constant.

(minimum) flow strength occurs shortly after the maximum (minimum) forcing (not shown). Second, the response curve of the circulation (Fig. 3) does not exhibit the qualitative structure of the response curve of the oscillator throughout the frequency range. For example, the flow strength simulated with the relatively small forcing period of 0.01 exhibits a relatively small amplitude (11%) compared to the amplitudes simulated for larger periods (Fig. 3). Whereas we do not have an explanation for the small amplitude for this particular experiment, the comparison illustrates that the analogy with the oscillator has limitations. Finally, the degree of asymmetry in the evolution of flow strength (e.g. Fig. 4a) varies also with the forcing frequency (not shown). Moreover, in an experiment similar to the reference experiment but with the non-linear terms removed from the equations of motion, the evolution of flow strength is apparently symmetric. Thus, the advection of vorticity and/or heat—in addition to the forcing frequency—seems to contribute to the asymmetric evolution. Albeit of interest in their own right, a detailed dynamical interpretation of the time-dependent flows (Figs. 3 and 4) is beyond the scope of this paper.

3.3. *Particle transport*

Particle transport is calculated in the time-dependent velocity fields $\mathbf{u} = \hat{x}u + \hat{z}w$ generated by the numerical model. The equations of particle transport in the isochoric 2-D flow are

$$\frac{dx}{dt} = +\frac{\partial \psi}{\partial z}, \tag{21}$$

$$\frac{dz}{dt} = -\frac{\partial \psi}{\partial x}. \tag{22}$$

Here $\mathbf{r} = \hat{x}x + \hat{z}z$ is the position of the particle in the container and ψ is the stream function of the flow, defined by $\mathbf{u} = \hat{y} \times \nabla\psi$. The finite-difference method used to solve eqs. 21 and 22 from the velocity fields generated by the numerical model is described in Appendix B.

Note the well-known analogy between the system (21–22) and Hamiltonian dynamics, with the stream function playing the role of the Hamiltonian H (Aref, 1984). The connection with Hamilton theory permits the following considerations about particle motion in the flow (e.g. Lichtenberg and Lieberman, 1983). First, the motion of a system with a time-dependent H is equivalent to that with a time-independent H with an additional degree of freedom. Thus, particle motion in a time-dependent 2-D flow is equivalent to that in a time-independent 3-D flow, that is, the mathematical properties of Lagrangian transport are expected to be similar in both types of flow. Second, a system with an autonomous H is 'integrable', whereas a system with H as an explicit function of time is not (integrability in the present context means that the Hamilton–Jacobi equation is separable into $\mathcal{N}$ independent equations, where $\mathcal{N}$ is the number of degrees of freedom). Thus, a regular motion of fluid particles is expected in a steady 2-D flow (where ψ is time-independent), whereas complicated particle motion may occur in an unsteady 2-D flow (where ψ is time-dependent).

We examine some characteristics of Lagrangian transport in the time-periodic flow of the reference experiment (Fig. 4). Two approaches are used to characterize the motion of particles in the

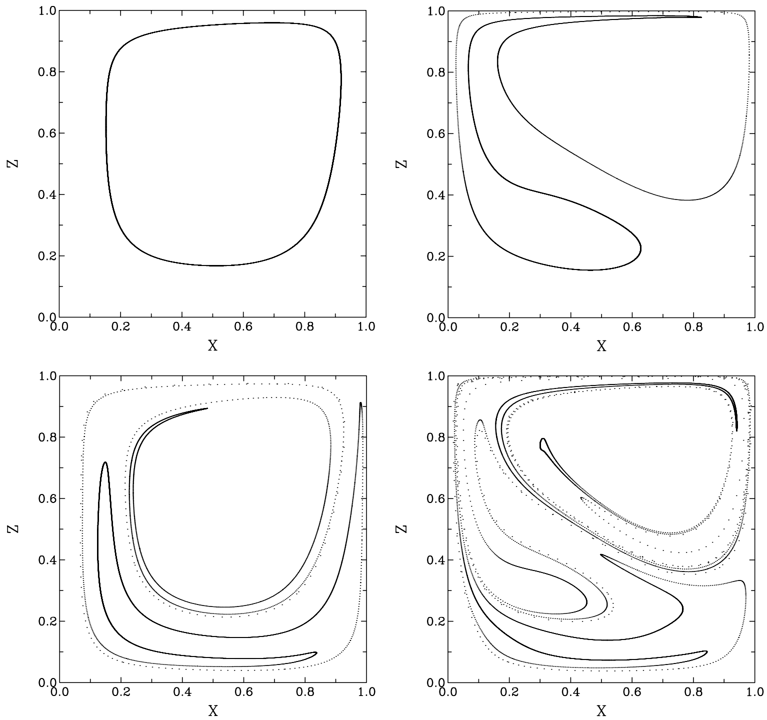

Fig. 5. Deformation of a line of particles in the reference experiment of time-periodic horizontal convection. The particles are initially positioned along a streamline (upper left panel). The line of particles is then continuously stretched and folded by the time-dependent flow (three other panels).

flow. Consider first the evolution of a line of a finite number of fluid particles, which approximates a material line as envisioned in theory (e.g. eq. 15). The particles composing the line are initially located along the same streamline (Fig. 5). This type of initial condition is guided by the fact that fluid particles move along streamlines in a steady flow. The separation of the computed particle trajectories from the streamline can thus be ascribed unambiguously to unsteadiness of the flow (within the accuracy of the finite-difference method used to compute particle transport; see Appendix B). It is found that the particle line becomes stretched and folded, tending to wrap the spatially variable vortex eye of the overturning cell (Fig. 5). The resulting structures are reminiscent of those observed in the laboratory for other time-dependent flows, such as time-periodic cavity flow (e.g. Ottino, 1989) and RB convection (e.g. Solomon et al., 1998). More generally, the stretching and folding of material lines (in 2-D flows) or material surfaces (in 3-D flows) may signify the presence of chaos (Ottino, 1989). Thus, chaotic particle transport may occur in the numerical flow.

To assess the presence of chaotic trajectories in the flow a Poincaré section is produced (e.g. Lichtenberg and Lieberman, 1983). A set of 10 particle trajectories is calculated. The position of each particle is strobed with a periodicity equal to the periodicity of the flow strength, or equivalently of the forcing (τ); the successive positions are then plotted on the same figure—the Poincaré section. A regular particle trajectory with a period τ would always be characterized by the same position in the Poincaré section, whereas a regular trajectory with a period 2τ would be identified by two different positions. More generally a regular trajectory with a period $n\tau$, where $n = 1, 2, \ldots$, would be characterized by n different positions. In contrast, an irregular trajectory would generally exhibit different positions, so that the Poincaré section for such trajectories would ultimately display a "chaotic sea". For reference a section obtained by sampling the particle positions in the steady flow with the same periodicity as for the time-dependent flow is also calculated (Fig. 6a). It is found from the Poincaré section for the time-periodic flow that the trajectories are irregular, the chaotic region occupying apparently the whole container (Fig. 6b).

Note that a chaotic sea does not characterize particle transport in all the time-dependent flows that we have generated. An example is provided by the flow simulated with the relatively low forcing period $\tau = 0.01$, for which the flow strength oscillates by only 11% (Fig. 3). The Poincaré map for this flow reveals drastic differences in particle transport between different regions of the fluid (Fig. 7). Conspicuous features in the map are closed curves that together form chains of "islands" (Fig. 7), which are characteristics of small perturbations of integrable systems (e.g. Lichtenberg and Lieberman, 1983). The presence of differences in mixing behaviour between different regions of the fluid suggests the presence of barriers to particle transport in the flow. The equivalent barriers in Hamiltonian systems are "KAM tori", which correspond to invariant curves on the Poincaré section. The existence of KAM tori is proven by the KAM theorem, provided that certain conditions are met. Nycander

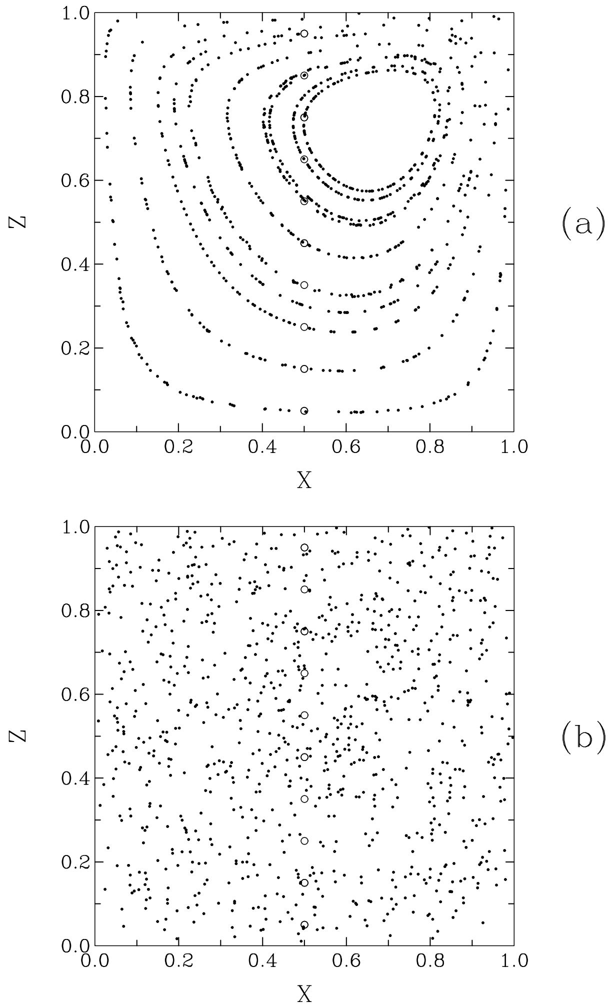

Fig. 6. Particle transport in numerical flows of horizontal convection. (a) Section computed by sampling the particle positions with a periodicity of 0.3 in the steady flow. (b) Poincaré section computed by strobing the particle positions with the same periodicity in a time-periodic flow with a forcing period $\tau = 0.3$ (reference experiment). For both flows the section is computed from the trajectory of 10 particles that initially are equally spaced along $x = 0.5$ (open circles).

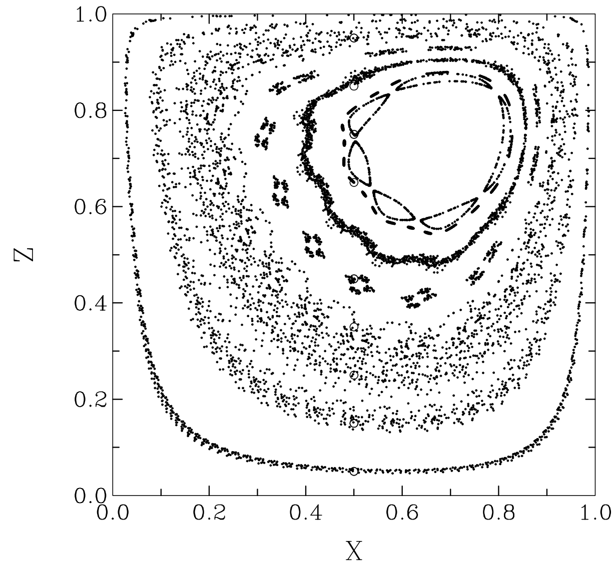

Fig. 7. Poincaré section computed by strobing particle positions with a periodicity of 0.01 in a time-periodic flow with a forcing period $\tau = 0.01$. The section is produced from the trajectory of 10 particles that initially are equally spaced along $x = 0.5$ (open circles).

et al. (2002) gave a useful interpretation of two conditions that are essential for the KAM theorem to hold. First, the mapping should be area preserving, that is, any closed curve should be mapped onto a closed curve with equal enclosed area. This condition is trivially met for the 2-D flow of an incompressible fluid. Second, the mapping should be continuously differentiable a sufficient number of time, for example, a smooth closed curve should be mapped onto another smooth closed curve. It is unclear whether this condition is met in our case: whereas the velocity field used to compute particle transport does not exhibit discontinuities, the spatial derivatives of this field does (Appendix B). Thus, the KAM tori in our case may not be perfect barriers to particle transport. Nycander et al. (2002) ascribed to this numerical artefact the "fuzziness" that is apparent in the Poincaré section for particles transport in an ocean general circulation model.

3.4. Flow structure

A question of pre-eminent interest to us concerns whether, despite chaotic particle transport, the path from the cold region to the warm region is below the return path (Jeffreys, 1925), as in the steady flow (Fig. 2). The balance equivalent to eq. (15) for the 2-D flow is

$$0 = Ra\left\langle \oint_m T\, dz \right\rangle + \left\langle \oint_m \left(\frac{\partial \omega}{\partial z}\, dx - \frac{\partial \omega}{\partial x}\, dz \right) \right\rangle. \tag{23}$$

The Jeffreys argument would be valid in unsteady flows if upward motion occurs in general in a warmer region of the container than downward motion, that is, if the term $Ra\ \langle \oint_m T dz \rangle$ is positive. This term can be expressed in another form by recognizing that the line integral of Tdz at some instant is the limit, as $\epsilon \to 0$, of the sum of contributions from a large number p of infinitesimal line elements of integration, each of length ϵ (e.g. Batchelor, 1967):

$$\begin{aligned} Ra\left\langle \oint_m T\, dz \right\rangle &= Ra\, \Delta t^{-1} \lim_{N\to\infty} \left\{ \sum_{k=1}^{N} \left(\oint_m T\, dz \right)_k \right\} \\ &= Ra\, \Delta t^{-1} \lim_{N\to\infty} \left\{ \sum_{k=1}^{N} \left(\lim_{\epsilon\to 0} \sum_p T_p \Delta z_p \right)_k \right\} \\ &= \Delta t^{-1} \lim_{N\to\infty} \left\{ \sum_p W_p(N) \right\}, \end{aligned} \tag{24}$$

where

$$W_p(N) = Ra \sum_{k=1}^{N} \lim_{\epsilon \to 0} (T_p \Delta z_p)_k \tag{25}$$

is the work done by buoyancy along the trajectory of the pth particle. If $Ra\langle \oint_m T dz \rangle > 0$, then $\sum_p W_p(N)$ must become positive. The time evolution of $\sum_p W_p(N)$, or equivalently of the average of $W_p(N)$, for all the particles composing the material line m, relates therefore to the flow structure of the unsteady flows. Below, the function $W_p(N)$ is computed for 100 particles that are initially positioned at random in the container and the time evolution of the average of $W_p(N)$ for the particle sample is examined (for details about the calculation of $W_p(N)$ see Appendix B).

For reference, consider first $W_p(N)$ and its average in the steady flow (thin lines in Fig. 8). In this flow, the function $W_p(N)$ is characterized by the superposition of an oscillation and a secular increase (Figs. 8a to c). The oscillation reflects the successive "revolutions" of the particles in the flow, whereas the secular increase indicates that the net work done by buoyancy on the particles over each revolution is positive; this work is balanced exactly by friction so that the circulation around each streamline is constant in time (eq. 19). The average of $W_p(N)$ for all particles increases almost linearly with time, the oscillatory components tending to cancel each other in the average (Fig. 8d). Perfect linearity would imply that the rate of work done by buoyancy on the particle sample, that is, the power developed by buoyancy forcing on the sample, is a constant of the flow.

Consider then $W_p(N)$ for particles positioned initially at the same locations but in the time-periodic flow of the reference experiment (thick lines in Fig. 8). As for the steady flow, the work done by buoyancy on individual particles increases generally with time (Figs. 8a to c). The average of $W_p(N)$ for all particles exhibits again a quasi linear increase (Fig. 8d): the bulk of particles moves up in the warm region and down in the cold region, and the rate of work done on the particle sample is about constant. Note that the average of $W_p(N)$ increases faster in the unsteady flow than in the steady flow, implying that buoyancy forcing is more effective at moving particles vertically in the unsteady flow.

It is thus concluded that, in spite of chaotic particle transport, the Jeffreys argument is valid for time-periodic 2-D flows of horizontal convection. The argument does not apply in this case to individual fluid elements but should be taken in the statistical sense only. It may apply to time-independent 3-D flows as well, given the similarity of the number of degrees of freedom for both types of flow (Section 3.3).

4. Summary

Jeffreys (1925) argued that the proper inference to draw from the Sandström theorem is that the path from the cold region to the warm region in a flow driven by a temperature contrast must lie below the return path. The argument can be formalized for a rotating fluid from three assumptions about the relative circulation around a closed material line: (1) the flow is steady; (2) the closed material line is a closed streamline and (3) the frictional work along the streamline is negative. It is valid for unsteady flows, that is, (1–2) can be relaxed, if the absolute circulation along the material line is a bounded function of time (eq. 15). Boundedness of the absolute circulation can easily be demonstrated for geophysical flows characterized by small Rossby number. By not relying on the assumptions of steadiness and streamline closedness, the relevance of the argument for the dynamical interpretation of geophysical flows is largely enhanced.

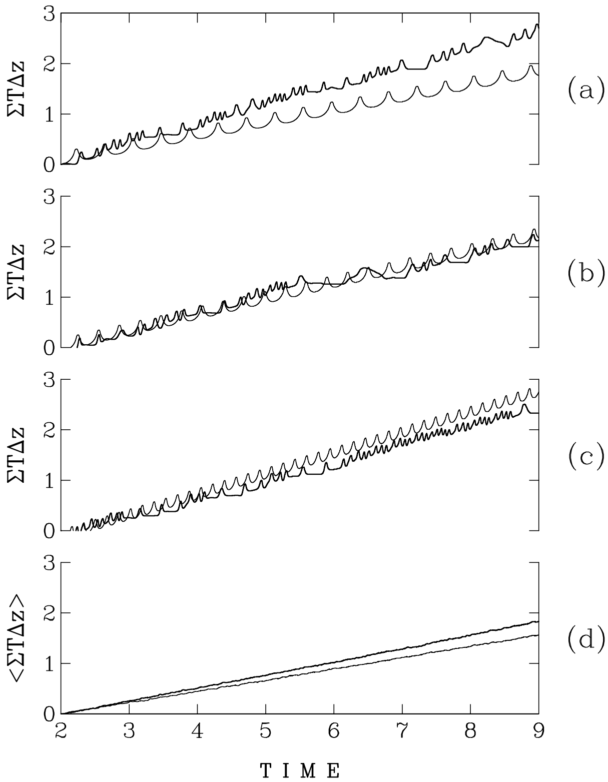

Fig. 8. Time-series of the work done by buoyancy (normalized to Ra) on fluid particles in the steady flow (thin lines) and in the time-periodic flow (thick lines). The work done on three individual particles from a sample of 100 particles that are initially positioned at random in the container is shown in panels (a–c). The work done on the whole particle sample (mean value) is shown in panel (d).

A further comment on the simple result (15) is in order. Taking eq. (15) as a support of the Jeffreys argument relies on the assumption that the frictional work along the moving material line is negative as $\Delta t \to \infty$. Note that it may be possible to find material lines along which the friction force at a given instant accelerates the fluid, because the velocities along these lines are less than in the neighbouring fluid (the same possibility exists for streamlines; see Dutton, 1986; p. 379). An ergodic argument, however, suggests that the time average of $\oint_m \mathbf{F} \cdot d\mathbf{r}$ should be negative if $\Delta t \to \infty$ in horizontal convection. Consider again a Newtonian incompressible fluid, for which $\mathbf{F} = \nu \nabla^2 \mathbf{u}$, with $\mathbf{u} = (u, v, w)$. The frictional work done on a fluid element over its displacement $d\mathbf{r} = \mathbf{u}\, dt$ has two distinct contributions, i.e., $\mathbf{F} \cdot d\mathbf{r} = (\mathbf{F} \cdot \mathbf{u})\, dt = (\nabla \cdot (\nu \nabla |\mathbf{u}|^2/2) - \nu |\nabla \mathbf{u}|^2)\, dt$. The first contribution arises from the divergence of the kinetic energy flux and the second contribution arises from the viscous dissipation of kinetic energy, where $|\nabla \mathbf{u}|^2 = \nabla u \cdot \nabla u + \nabla v \cdot \nabla v + \nabla w \cdot \nabla w$ is the deformation (positive definite). During the infinitesimal time interval dt, the work done by friction over the whole fluid is, by virtue of the divergence theorem,

$$\int \rho_0 \mathbf{F} \cdot d\mathbf{r}\, dV = dt \int \left(\rho_0 \nu \nabla \frac{|\mathbf{u}|^2}{2} \right) \cdot \hat{n}\, dS - dt \int \rho_0 \nu |\nabla \mathbf{u}|^2\, dV, \tag{26}$$

where dV is a volume element and dS is a surface element at the fluid boundary with outward unit vector $\hat{n}$. A constant density ρ_0 is inserted in eq. (26) so that each term has units of energy. The integrand of the first term on the right-hand side is $\rho_0 \nu \nabla |\mathbf{u}|^2/2 \cdot \hat{n} = \rho_0 \nu |\mathbf{u}| \partial |\mathbf{u}| / \partial n$, where $\partial/\partial n \equiv \hat{n} \cdot \nabla$. If a condition of no slip and/or no stress applies at the fluid boundaries, this term vanishes, so that the volume integral (or average) of $\rho_0 \mathbf{F} \cdot d\mathbf{r}$ (or $\mathbf{F} \cdot d\mathbf{r}$) is negative once the fluid is in motion. Now suppose that the trajectories of the particles are "space filling", so that an arbitrary line of particles tends to sample the whole volume of the fluid. In this case, the time average of $\oint_m \mathbf{F} \cdot d\mathbf{r}$ when $\Delta t \to \infty$ should be negative as the volume average of $\mathbf{F} \cdot d\mathbf{r}$ is negative at all instants.

Our numerical study verifies this ergodic argument for time-periodic 2-D horizontal convection. When the flow variability is sufficiently large, the Poincaré section suggests the presence of a chaotic sea, that is, fluid particles tend to sample the whole container. In this regime, the ergodic argument suggests that $\langle \oint_m \mathbf{F} \cdot d\mathbf{r} \rangle < 0$ for $\Delta t \to \infty$. It was shown that, in spite of chaoticness, fluid particles experience in general a secular increase in buoyancy forcing (section 3.4): in general, the particles exhibit upward motion in the warm region and downward motion in the cold region of the fluid. Thus, $Ra \langle \oint_m T\, dz \rangle$ should be positive for $\Delta t \to \infty$, which supports the Jeffreys argument. Combining this result with the circulation balance eq. (15) implies that $\langle \oint_m \mathbf{F} \cdot d\mathbf{r} \rangle$ should be negative for $\Delta t \to \infty$, which supports the ergodic argument. Because a time-dependent 2-D flow and a time-independent 3-D flow have the same number of degrees of freedom, the Jeffreys argument may be valid in the latter flow type as well.

There are interesting apparent similarities in the qualitative properties of particle transport for time-dependent horizontal convection as determined in this work and for other simple time-dependent flows that have been more extensively studied. A time-periodic flow that has received particular attention from the viewpoint of particle motion is the even oscillatory instability of RB convection, where the roll boundaries undergo a collective oscillation in the direction perpendicular to the roll axes. Computer simulations for the 2-D case suggest that the basic mechanism of particle transport is chaotic advection in the vicinity of the roll boundaries (Solomon and Gollub, 1988). Thus, chaotic particle motion can occur in laminar time-dependent 2-D convection, whenever the flow is forced by a horizontal temperature contrast (this study) or a vertical temperature contrast. The structures that develop during the evolution of a line of particles (Fig. 5) are reminiscent of the "lobes" that form at the roll boundaries in laboratory experiments of RB convection (e.g. Solomon et al., 1996, 1998). These lobes become stretched and folded, as for the particle line (Fig. 5). Camassa and Wiggins (1991) proposed a transport theory for 2-D RB convection in the regime of even oscillatory instability. In this theory the stretching and folding of lobes is a primary mechanism by which fluid is exchanged from roll to roll—a prediction that is consistent with experimental results (e.g. Solomon et al., 1996). From the theory analytical estimates of different quantities of physical interest have been derived, such as the size and location of islands and KAM tori for the Poincaré map (Camassa and Wiggins, 1991). Experimental evidence for the existence of KAM barriers in RB convection has been reported (e.g. Solomon et al., 1996, 1998). It is hoped that the present investigation will stimulate future work on these and other elements of particle transport in horizontal convection.

It is perhaps worth being explicit about some of the limitations of this paper. First, it is limited to one specific inference from the Sandström theorem (Jeffreys, 1925). Lines of research prompted by other interpretations of the theorem, such as the overall question of how much circulation results from a given thermal forcing (e.g. Paparella and Young, 2002; Siggers et al., 2004), are outside the scope of this paper which deals with the shape—not the intensity—of horizontal convection. Second, the effects on particle transport of a stress applied at the fluid boundaries have not been investigated in the present study focused on purely buoyancy-forced flows. It is unclear whether taking eq. (15) as a foundation to the Jeffreys argument is valid for the general case where the fluid is both thermodynamically and mechanically forced. When a stress is imposed to the fluid, the volume integral of the frictional power $\mathbf{F} \cdot \mathbf{u}$ may be positive if the net flux of kinetic energy supplied to the fluid at its boundaries exceeds the viscous dissipation. Current uncertainties in the energy budget of the global ocean (e.g. Wunsch and Ferrari, 2004) suggest that attempting to determine whether this is the case for the oceanic fluid is premature. Finally, our numerical study of particle transport (Section 3) suffers from several limitations with regard to its implications for geophysical flows. The greatest drawbacks are probably the assumption of two-dimensionality, the absence of rotation, and the lack of dynamical similarity between the flows simulated by the numerical model and the large-scale meridional flows that are inferred to occur in the ocean. It is unclear how our numerical results could be extrapolated to time-dependent 3-D flows or to flows where the velocity field itself is chaotic (turbulent). Eddying flows have been shown to arise spontaneously in horizontal convection in experimental studies (e.g. Miller, 1968; Mullarney et al., 2004) and in numerical simulations (e.g. Paparella and Young, 2002). The flow regimes accessed in laboratory and numerical studies of horizontal convection are well removed from the oceanic conditions. Most notably, the Rayleigh number characterizing the planetary-scale uneven heating at the sea surface is huge: a buoyancy contrast $\sim 10^{-2}$ m s^{-2} imposed on a water layer with a thickness $\sim 10^3$ m corresponds to a Rayleigh number on order of 10^{20}. Approaching a thermal driving of this magnitude represents a challenge in experiments of horizontal convection.

5. Acknowledgements

We thank Alain Colin de Verdière and Jonas Nycander for very helpful discussions and comments. The constructive remarks by the anonymous reviewers improve the manuscript and are acknowledged. The fact that eq. (14) leads to eq. (15) if the absolute circulation is bounded has been brought to our attention by an anonymous reviewer. Discussions with Robert Beardsley, Rui Xin Huang, Mahdi Ben Jelloul, Lawrence Pratt, Rob Scott, Michael Spall and Carl Wunsch have also been helpful. This work has been supported in part by a grant from the U.S. National Science Foundation.

6. Appendix A. Numerical model of horizontal convection

This appendix describes the numerical model of horizontal convection used in this work. Whereas the model is identical to that used in earlier studies (e.g. Beardsley and Festa, 1972; Rossby, 1998), our method of solution is slightly different. We consider the flow in a vertical plane of a Boussinesq fluid forced only by a temperature contrast imposed at the top. The velocity vector has only two components, $\mathbf{u} = \hat{x}u + \hat{z}w$, and the fluid is taken as incompressible, $\nabla_2 \cdot \mathbf{u} = 0$, and Newtonian, $\mathbf{F} = \nu\nabla_2^2\,\mathbf{u}$, where $\nabla_2 = \hat{x}\partial/\partial x + \hat{z}\partial/\partial z$. A stream function ψ is thus introduced, $\mathbf{u} = \hat{y} \times \nabla_2\psi$. Rotation is omitted. The equations of motion are:

$$\frac{\partial \omega}{\partial t} = J(\psi, \omega) - g\alpha\frac{\partial T}{\partial x} + \nu\nabla_2^2\omega, \tag{A1}$$

$$\frac{\partial T}{\partial t} = J(\psi, T) + \kappa\nabla_2^2 T. \tag{A2}$$

Here $\omega = \hat{y} \cdot (\nabla_2 \times \mathbf{u})$ is the vorticity, T is the temperature, t is time, $J(a, b) = \partial a/\partial x\, \partial b/\partial z - \partial a/\partial z\, \partial b/\partial x$ is the Jacobian operator, g is the acceleration due to gravity, α is the coefficient of thermal expansion, ν is the kinematic viscosity, and κ is the thermal diffusivity. The stream function and the vorticity are related through a Poisson equation:

$$\nabla_2^2\psi = \omega. \tag{A3}$$

The equations are non-dimensionalized by introducing the following relations:

$$t = \frac{L^2}{\kappa}t_*, \tag{A4}$$

$$(x, z) = L\,(x_*, z_*)\,, \tag{A5}$$

$$\omega = \frac{k}{L^2}\omega_*, \tag{A6}$$

$$T = \Delta T\, T_*, \tag{A7}$$

$$\psi = k\psi_*, \tag{A8}$$

where L is the dimension of the container and ΔT is proportional to the temperature difference imposed at the surface. The vertical and horizontal dimensions of the container are the same, that is, the aspect ratio is equal to one. Quantities with subscript * are dimensionless.

The dimensionless equations of motion are (omitting subscript * for clarity):

$$\frac{\partial \omega}{\partial t} = J(\psi, \omega) + Pr\left(-Ra\frac{\partial T}{\partial x} + \nabla_2^2\omega\right), \tag{A9}$$

$$\frac{\partial T}{\partial t} = J\,(\psi, T) + \nabla_2^2 T, \tag{A10}$$

where $Ra = g\alpha\Delta T L^3/(\nu\kappa)$ is the Rayleigh number and $Pr = \nu/\kappa$ is the Prandtl number. The relation between the stream function and the vorticity is identical in form to (A3). The governing eqs. (A9–A10) and the Poisson equation $\nabla_2^2\psi = \omega$ are solved with an isothermal fluid at rest as initial conditions ($\omega = \psi = T = 0$) and with the following boundary conditions: (1) no normal flow at all boundaries, (2) no slip at the bottom and side boundaries, (3) no stress at the top boundary, (4) no heat flux at the bottom and side boundaries, and (5) a temperature distribution along the top boundary.

Our method of solution assumes a square grid where the grid nodes carry the values of ω, T and ψ (Fig. 9). All boundaries coincide with grid nodes. Thus, the following indexing scheme is used:

$$x_i = i\Delta x, \qquad i = 0, 1, \ldots, I, \tag{A11}$$

$$z_j = j\Delta z, \qquad j = 0, 1, \ldots, J, \tag{A12}$$

$$t_n = n\Delta t, \qquad n = 0, 1, \ldots, \tag{A13}$$

where $\Delta x = I^{-1}$ ($\Delta z = J^{-1}$) is the distance between two adjacent nodes along the coordinate x (z) and Δt is the time step. Here $\Delta x = \Delta z = \Delta$. The grid size $\Delta = 50^{-1}$; in the numerical flows for which particle transport is computed $\Delta = 100^{-1}$. The indexes 0, I and J denote variables on the boundaries.

The equations of motion are solved numerically as follows. The buoyancy term in (A9) is approximated by a central

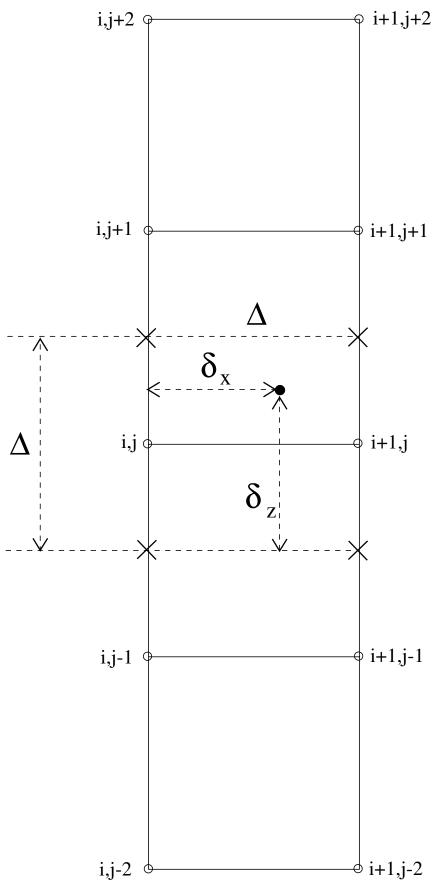

Fig. 9. Grid of the numerical model of horizontal convection. The dynamical variables (ω, ψ, T) are defined at the grid nodes (open circles). The partial derivatives $\partial\psi/\partial z$ and $-\partial\psi/\partial x$ which are evaluated to compute particle transport are defined at the intermediate points (crosses). The figure shows the grid nodes that are considered in the evaluation of $\partial\psi/\partial z$ at the intermediate points $i,\ j \pm \frac{1}{2}$ and $i+1,\ j \pm \frac{1}{2}$ (Appendix B). The quantities δ_x and δ_z are distances used to compute the transport of the particle (solid circle). The size of the grid cells is Δ.

difference scheme, whereas the diffusion terms in (A9–A10) are discretized by the usual five-point formula. A Dufort–Frankel scheme is used for the temporal derivatives and the diffusion terms. The finite difference analogues of the differential eqs. (A9–A10) are thus:

$$\begin{aligned}\frac{\omega_{ij}^{n+1} - \omega_{ij}^{n-1}}{2\Delta t} &= J_d(\psi^n, \omega^n)_{ij} \\ &\quad - \frac{Pr\,Ra}{2\Delta}\left(T_{i+1j}^n - T_{i-1j}^n\right) \\ &\quad + \frac{Pr}{\Delta^2}\left(\omega_{i+1j}^n + \omega_{i-1j}^n + \omega_{ij-1}^n + \omega_{ij+1}^n - 2\omega_{ij}^{n-1} - 2\omega_{ij}^{n+1}\right),\end{aligned} \tag{A14}$$

$$\begin{aligned}\frac{T_{ij}^{n+1} - T_{ij}^{n-1}}{2\Delta t} &= J_d(\psi^n, T^n)_{ij} \\ &\quad - \frac{1}{\Delta^2}\left(T_{i+1j}^n + T_{i-1j}^n + T_{ij-1}^n + T_{ij+1}^n - 2T_{ij}^{n-1} - 2T_{ij}^{n+1}\right).\end{aligned} \tag{A15}$$

For the Jacobian for vorticity, $J_d(\psi^n, \omega^n)_{ij}$, we use the finite difference form $(J_{++} + J_{+\times} + J_{\times+})/3$ of Arakawa (1966). This form satisfies the mathematical property $J(a, b) = -J(b, a)$ and ensures that the mean kinetic energy and mean square vorticity over the computational domain are conserved in the appropriate limits. For the Jacobian for temperature, $J_d(\psi^n, T^n)_{ij}$, the finite difference form $J_{\times+}$ is employed (Arakawa, 1966), which guarantees that the mean temperature and mean square temperature are conserved in the appropriate limits. Note that the finite-difference forms (A14–A15) require knowledge of ω_{ij} and T_{ij} at the two previous time levels, whereas initial conditions are provided at only one time. Here a simple forward step is used to initialize the three-level eqs. (A14–A15). The value of Δt used for numerical integration is checked at each time level for numerical stability (CFL criterion). Finally the elliptic problem for ψ, $\nabla_2^2\psi = \omega$, is solved from the five-point formula:

$$\psi_{i+1j}^n + \psi_{i-1j}^n + \psi_{ij+1}^n + \psi_{ij-1}^n - 4\psi_{ij}^n = \Delta^2\,\omega_{ij}^n. \tag{A16}$$

The discrete values ψ_{ij} are obtained using a Fourier transform method (Press et al., 1992; p. 850). A variant of the fast Fourier transform algorithm is used.

The numerical implementation of the boundary conditions is as follows. The condition of no normal flow at the boundaries is satisfied by prescribing a constant value (namely, zero) to the stream function at the boundaries. The condition of no slip at the bottom and side boundaries is expressed as a condition on the vorticity (e.g. Roache, 1982; p. 141). Consider the vorticity condition at the left boundary. A Taylor expansion of the stream function at a distance Δx from this boundary gives:

$$\psi_{1j} = \psi_{0j} + \left(\frac{\partial\psi}{\partial x}\right)_{0j}\Delta x + \left(\frac{\partial^2\psi}{\partial x^2}\right)_{0j}\frac{(\Delta x)^2}{2} + \mathcal{O}(\Delta x)^3. \tag{A17}$$

Now, $(\partial\psi/\partial x)_{0j} = -w_{0,j} = 0$ from the condition of no slip at the boundary and $(\partial\psi^2/\partial x^2)_{0j} = -(\partial w/\partial x)_{0j}$. The vorticity at the boundary $\omega_{0j} = (\partial u/\partial z)_{0j} - (\partial w/\partial x)_{0j} = -(\partial w/\partial x)_{0j}$ from the condition of no normal flow. Thus, the vorticity at the left boundary is given by

$$\omega_{0j} = 2\frac{\psi_{1j}}{(\Delta x)^2}, \tag{A18}$$

which is accurate to first order. A similar expression is used at the bottom and right boundaries. The condition of no stress at the top boundary is also expressed as a condition on the vorticity:

$$\omega_{iJ} = \left(\frac{\partial u}{\partial z}\right)_{iJ} - \left(\frac{\partial w}{\partial x}\right)_{iJ} = \left(\frac{\partial u}{\partial z}\right)_{iJ} = 0. \tag{A19}$$

The second equality follows from the condition of no normal flow. The condition of no heat flux at the side and bottom boundaries is satisfied by equating the temperature at the boundary to the temperature at the first inner grid node in the direction normal to the boundary. Finally, different temperature distributions are imposed at the top boundary, as described in the main text.

The accuracy and convergence of the method of solution are assessed as follows. To assess the method accuracy we compare (1) the quasi steady-state field of temperature simulated by the numerical model in the linear limit ($J(a, b) = 0$) with (2) the temperature field obtained from the analytical solution of the Laplace equation $\nabla_2^2 T = 0$ with the same thermal boundary conditions, that is,

$$T(x, z) = \frac{1}{2} + \sum_{\mathrm{odd\,n}}^{\infty} \left(\frac{2}{n\pi}\right)^2 \frac{\cosh(n\pi z)}{\cosh(n\pi)} \cos(n\pi x). \tag{A20}$$

The mean absolute difference between the field simulated with the grid spacing $\Delta = 50^{-1}$ ($\Delta = 100^{-1}$) and the analytical field averages 2.0×10^{-3} (1.0×10^{-3}), which is small compared to the temperature range between 0 and 1. To assess the convergence we compare visually the quasi steady-state fields of vorticity, temperature, and stream function simulated with $\Delta = 50^{-1}$ and $\Delta = 100^{-1}$. Differences between the two simulations are generally very small (not shown).

7. Appendix B. Computation of particle transport

This appendix describes (1) the method of solution of the ordinary differential equations for particle transport (eqs. 21–22 in the text) and (2) the calculation of the work done by buoyancy on individual particles along their trajectories (eq. 25). Eqs. (21–22) are solved numerically using a fourth-order Runge–Kutta scheme for time integration (with a value for the time step Δt similar to the one used to integrate the equations of fluid motion; see Appendix A). The partial derivatives $\partial\psi/\partial z$ and $-\partial\psi/\partial x$ are estimated as follows. Consider the estimation of $\partial\psi/\partial z$ for a particle located in a grid cell whose nodes carry the values ψ_{ij}, ψ_{ij+1}, ψ_{i+1j+1}, and ψ_{i+1j} (Fig. 9). A fourth-order central difference scheme is used to provide an approximation of $\partial\psi/\partial z$ at the intermediate points $(i, j \pm \frac{1}{2})$ and $(i + 1, j \pm \frac{1}{2})$. For example, $\partial\psi/\partial z$ at $(i, j - \frac{1}{2})$ is approximated by

$$\frac{-\psi_{ij+1} + 27\psi_{ij} - 27\psi_{ij-1} + \psi_{ij-2}}{24\Delta}. \tag{B1}$$

An estimate of $\partial\psi/\partial z$ at the particle position is then given by linearly interpolating the estimates of $\partial\psi/\partial z$ at the intermediate points. For example, the contribution of $\partial\psi/\partial z$ at point $(i, j - \frac{1}{2})$ to $\partial\psi/\partial z$ at the particle position is $(\Delta - \delta_x)(\Delta - \delta_z)/\Delta^2 \cdot$ (B1), where δ_x (δ_z) is a horizontal (vertical) distance (Fig. 9). A similar approach is used to estimate $-\partial\psi/\partial x$ at the particle position.

Note that the four-point formula (B1) cannot be used if the particle is near a boundary. If the particle is positioned at a distance $\leq 3\Delta/2$ from a boundary, $\partial\psi/\partial z$ and $-\partial\psi/\partial x$ at the intermediate positions are approximated by a second-order central difference scheme and the partial derivatives at the particle location are again obtained by linear interpolation. For example, if $j = 0$, $\partial\psi/\partial z$ at location $(i, \frac{1}{2})$ is approximated by

$$\frac{\psi_{i1} - \psi_{i0}}{\Delta}. \tag{B2}$$

The partial derivative $\partial\psi/\partial z$ at the particle position is then given by linearly interpolating between this value and $\partial\psi/\partial z$ at $(i + 1, \frac{1}{2})$. The contribution from the intermediate point $(i, \frac{1}{2})$ is then given by $(\Delta - \delta_x)/\Delta \cdot$(B2), where δ_x is the distance of the particle from the left boundary of the grid cell.

The accuracy of the finite-difference method for particle transport is tested in two ways. First, a particle is positioned initially on an arbitrary streamline in the steady flow ("+" in Fig. 2). Because the flow is steady, the advected particle should remain exactly on the streamline if the finite-difference method were perfectly accurate. The particle remains almost exactly on the streamline and comes back very close to its initial position after about one revolution in the flow (compare "+" and large dot in Fig. 2). A more stringent test is provided by strobing at relatively small frequency the position of a set of particles placed in the steady flow (Fig. 6a). After a large number of revolutions in the flow, the individual particles remain very close to the streamlines on which they were initially positioned. Although departures between a given pathline and the corresponding streamline do exist, these are relatively small. Thus, the finite-difference method used to calculate particle transport is deemed to give sufficiently accurate results for our purpose.

The work done by the buoyancy force on a given fluid particle along its trajectory (eq. 25) is computed from the mean temperature of the grid cells occupied by the particle and the changes in the vertical coordinate of the particle:

$$W_p(N) = Ra \sum_{k}^{N} \left(\frac{T_O + T_N}{2} (z_N - z_0) \right)_k. \tag{B3}$$

Here $T_O(T_N)$ is the mean temperature of the grid cell that harbours the particle before (after) the kth displacement from the old vertical position z_O to the new vertical position z_N. For example, for a particle that is initially located in the grid cell shown in Fig. 9,

$$T_O = \frac{T_{ij} + T_{ij+1} + T_{i+1j+1} + T_{i+1j}}{4}. \tag{B4}$$

References

Arakawa, A. 1966. Computational design for long-term numerical integration of the equations of fluid motion: two dimensional incompressible flow. Part I. *J. Comp. Phys.* **1**, 119–143.

Aref, H. 1984. Stirring by chaotic advection. *J. Fluid Mech.* **143**, 1–21.

Batchelor, G. K. 1967. *An Introduction to Fluid Dynamics.* Cambridge University Press, Cambridge, 615 p.

Beardsley, R. C. and Festa, J. F. 1972. A numerical model of convection driven by a surface and non-uniform horizontal heating. *J. Phys. Oceanogr.* **2**, 444–455.

Camassa, R. and Wiggins, S. 1991. Chaotic advection in a Rayleigh-Bénard flow. *Phys. Rev. A* **43**, 774–797.

Colin de Verdière, A. 1993. On the oceanic thermohaline circulation. In: *Modeling Oceanic Climate Interactions* (eds. J. Willebrand, and D. L. T. Anderson), pp. 151–183, NATO ASI Series, Vol. I11.

Defant, A. 1961. *Physical oceanography.* Vol. I. Pergamon Press, New York, 729 pp.

Dutton, J. A. 1986. *The Ceaseless Wind: An Introduction to the Theory of Atmospheric Motion*, Dover Publications, Inc., New York, 617 p.

Gade, H. G. and Gustafsson, K. E. 2004. Application of classical thermodynamical principles to the study of the oceanic overturning circulation. *Tellus* **56A**, 371–386.

Godske, C. L. 1936. Note on the apparent discrepancy between Bjerknes-Sandström and H. Jeffreys. *Q. J. Roy. Met. Soc.* **62**, 446–449.

Godske, C. L., Bergeron, T., Bjerknes, J. and Bundgaard, R. C. 1957. *Dynamic Meteorology and Weather Forecasting.* American Meteorological Society, Boston, USA, 800 p.

Huang, R. X. 1999. Mixing and energetics of the ocean thermohaline circulation. *J. Phys. Oceanogr.* **29**, 727–746.

Jeffreys, H. W. 1925. On fluid motions produced by differences of temperature and humidity. *Q. J. Roy. Met. Soc.* **51**, 347–356.

Jeffreys, H. W. 1936. Note on Dr. Godske's paper. *Q. J. Roy. Met. Soc.* **62**, 449–450.

Lichtenberg, A. J. and Lieberman, M. A. 1983. *Regular and Stochastic Motion*. Series in Applied Mathematical Sciences, Vol. 38, Springer-Verlag, New York, 499 p.

Miller, R. C. 1968. *A Thermally Convecting Fluid Heated Non-Uniformly from Below: An Experimental Study*. Ph.D, M.I.T.

Mullarney, J. C., Griffiths, R. W. and Hughes, G. O. 2004. Convection driven by differential heating at a horizontal boundary. *J. Fluid Mech.* **516**, 181–209.

Munk, W. and Wunsch, C. 1998. Abyssal recipes II: energetics of tidal and wind mixing. *Deep Sea Res.* **45**, 1977–2010.

Nycander, J., Döös, K. and Coward, A. C. 2002. Chaotic and regular trajectories in the Antarctic Circumpolar Current. *Tellus, Ser. A* **54**, 99–106.

Ottino, J. M. 1989. *The Kinematics of Mixing: Stretching, Chaos, and Transport*. Cambridge University Press, Cambridge, 364 p.

Ottino, J. M. 1990. Mixing, chaotic advection, and turbulence. *Ann. Rev. Fluid Mech.* **22**, 207–253.

Paparella, F. and Young, W. R. 2002. Horizontal convection is non-turbulent. *J. Fluid Mech.* **466**, 205–214.

Pedlosky, J. 1987. *Geophysical Fluid Dynamics*. 2nd Edition, Springer, New York, 710 p.

Press, W. H., Teukolsky, S. A., Vetterling, W. T. and Flannery, B. P. 1992. *Numerical Recipes (in Fortran)—The Art of Scientific Computing*. 2nd Edition, Cambridge University Press, Cambridge, 963 p.

Roache, P. J. 1982. *Computational Fluid Dynamics*. Hermosa Publishers, Albuqueque, 446 p.

Rossby, T. 1998. Numerical experiments with a fluid heated non-uniformly from below. *Tellus* **50A**, 242–257.

Sandström, J. W. 1916. Meteorologische Studien im schwedischen Hochgebirge. *Göteborgs K. Vetenskaps- och Vitterhetssamhälles Handl. (Gothenburg, Sweden)* **22**, 48 p.

Siggers, J. H., Kerswell, R. R. and Balmforth, N. J. 2004. Bounds on horizontal convection. *J. Fluid Mech.* **517**, 55–70.

Solomon, T. H. and Gollub, J. P. 1988. Chaotic particle transport in time-dependent Rayleigh-Bénard convection. *Phys. Rev. A* **38**, 6280–6286.

Solomon, T. H., Tomas, S. and Warner, J. L. 1996. Role of lobes in chaotic mixing of miscible and immiscible impurities. *Phys. Rev. Lett.* **77**, 2682–2685.

Solomon, T. H., Tomas, S. and Warner, J. L. 1998. Chaotic mixing of immiscible impurities in a two-dimensional flow. *Phys. Fluids* **10**, 342–350.

Stern, M. E. 1975. *Ocean Circulation Physics.* Academic Press, New York.

Wang, W. and Huang, R. X. 2005. An experimental study of thermal circulation driven by horizontal differential heating. *J. Fluid Mech.* **540**, 49–73.

Wunsch, C. 2005. Thermohaline loops, Stommel box models, and the Sandström theorem. *Tellus* **57A**, 84–99.

Wunsch, C. and Ferrari, R. 2004. Vertical mixing, energy, and the general circulation of the oceans. *Ann. Rev. Fluid Mech.* **36**, 281–313.